Extremely Efficient Indium–Tin-Oxide-Free Green Phosphorescent Organic Light-Emitting Diodes

Min Cai, Zhuo Ye, Teng Xiao, Rui Liu, Ying Chen, Robert W. Mayer, Rana Biswas, Kai-Ming Ho, Ruth Shinar, and Joseph Shinar**

The rapid development of organic light-emitting diodes (OLEDs) in recent years makes them increasingly competitive in flat-panel display and solid state lighting applications.[1–3] In particular, using phosphorescent molecules as the emitters allows for efficient light emission from both excited singlet and triplet states, which can lead to a nearly 100% internal quantum efficiency η_{int}.[4–6] The external quantum efficiency η_{ext} is related to η_{int} and the outcoupling efficiency η_{out} (the fraction of light that is outcoupled in the forward direction) by the following relation:

$$\eta_{ext} = \eta_{int}\eta_{out} \quad (1)$$

Hence, the greatest potential for a substantial increase in OLEDs' efficiencies is to enhance η_{out} and indeed, various approaches aimed at achieving this have been reported. These include the use of a scattering medium, microlens arrays (μLAs), nanoparticles and nanostructures, photonic crystals, microcavities and nanocavities, modified substrates, and surface plasmons.[7–9]

The basic device structure of a conventional bottom-emitting OLED consists of multiple organic layers situated between two electrodes, the anode and cathode, all deposited on a substrate, typically glass.[10] An OLED requires at least one transparent electrode in order to emit light. Indium tin oxide (ITO) is currently the dominant transparent anode; it is optically transparent in most of the visible range and has good electrical conductivity.[11] However, it presents several key issues: (1) its relatively high index of refraction ($n_{ITO} \sim 2.0$), which is higher than $n_{org} \sim 1.7$ of the organic materials and $n_{gl} \sim 1.5$ of the conventional glass substrate. These differences in n cause unwanted total internal reflection (TIR) at the ITO/glass interface,[7] (2) its deposition process is relatively inefficient,[12–13] (3) it is fragile and inflexible due to its ceramic nature, which limits the processing advantages of organic materials,[14–15] and (4) its surface is relatively rough, which could cause contact problems and energy loss.[11] Thus, these issues beg for alternatives, and conducting polymers,[16–19] carbon nanotubes,[20] graphene,[21] thin metal layers[22] and printable metal grids[23] are being investigated for this purpose.

Poly(3,4-ethylene dioxythiophene):poly(styrene sulfonate) (PEDOT:PSS; $n_{PEDOT:PSS} \sim 1.5$),[16,24] which is extensively used as a buffer layer between ITO and the organic layers in organic devices,[10,25] is a promising organic electrode material. This is due to its conductivity $\sigma_{PEDOT:PSS}$ that drastically increases to > 1000 S cm^{-1} by depositing it from mixed solutions prepared by adding solvents with higher boiling points than water into the aqueous PEDOT:PSS solution. Suitable solvents include dimethyl sulfoxide, N,N-dimethylformamide, sorbitol, glycerol, and ethylene glycol (EG).[11,16–19,25–26] In particular, recent studies showed that the increase in $\sigma_{PEDOT:PSS}$ can be achieved not only by mixing EG with aqueous PEDOT:PSS, but also by immersing PEDOT:PSS films in an EG solution for a few minutes.[18–20,25,27] With such highly conductive PEDOT:PSS anodes, improved OLEDs (relative to devices with ITO) have been reported,[16,19] and the improved performance is commonly assigned to optical enhancement due to the advantageous optical properties of PEDOT:PSS anode, which is nearly index matched to glass. However, to our knowledge, a careful analysis of the origin of this optical enhancement has not been reported.

In this paper, we demonstrate extremely efficient ITO-free green phosphorescent OLEDs (PHOLEDs) with multilayered, highly conductive PEDOT:PSS anodes on a glass substrate. The structure of these PHOLEDs is glass/PEDOT:PSS/MoO_3/MoO_3 (10 wt.%):NPD/NPD/Ir(ppy)$_3$ (6 wt%):CBP/BPhen/LiF/Al, where NPD is N,N'-diphenyl-N,N'-bis(1-naphthyl-phenyl)-1,1'-biphenyl-4,4'-diamine, CBP is 4,4'-bis(9-carbazolyl)-biphenyl, Ir(ppy)$_3$ is tris(2-phenylpyridine) iridium(III) and BPhen is 4,7-diphenyl-1,10-phenanthroline (see Figure S1 in Supporting Information (SI) for device and material structures). Peak luminous efficiency $\eta_{L,max} = 127$ Cd A^{-1}, peak power efficiency $\eta_{P,max} = 118$ lm W^{-1} and peak external quantum efficiency $\eta_{ext,max} = 40\%$ are achieved without any outcoupling-enhancing structures. These values are among the highest reported for ITO-free OLEDs and are significantly higher than those of the otherwise identical devices with ITO anodes fabricated on identical glass substrates under nominally identical conditions. Importantly, a quantitative optical simulation is described, revealing that the optical enhancement is due mainly to a weak microcavity effect, specifically, the suppression of waveguide modes in PEDOT:PSS-anode OLEDs.

Figure 1 shows the transmittance T at 550 nm (T_{550}) and sheet resistance R_S of the multilayered, highly conductive

Dr. M. Cai, Dr. T. Xiao, Dr. Z. Ye, R. Liu, Dr. Y. Chen, Prof. K.-M. Ho, Prof. J. Shinar
Ames Laboratory-USDOE and Department of Physics and Astronomy
Iowa State University
Ames, IA 50011, USA
E-mail: jshinar@iastate.edu; rshinar@iastate.edu
R. W. Mayer, Prof. R. Biswas, Prof. R. Shinar
Microelectronics Research Center and Department of Electrical and Computer Engineering
Iowa State University
Ames, IA 50011, USA
E-mail: rshinar@iastate.edu; jshinar@iastate.edu

DOI: 10.1002/adma.201202035

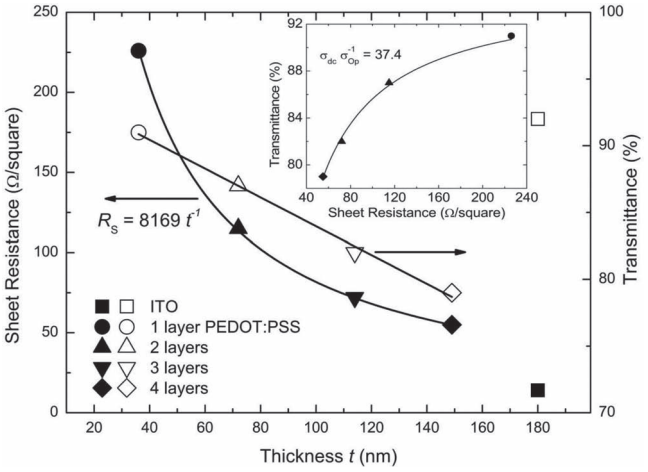

Figure 1. The transmittance T_{550} and sheet resistance R_S for ITO and multilayered PEDOT:PSS films as a function of film thickness. The PEDOT:PSS R_S values are in excellent agreement with $R_S = R_0 t^{-1}$, yielding $R_0 = 8170\ \Omega\ sq^{-1}$. Inset: T_{550} vs R_S. The solid line is the best fit of Equation (2), which yields $\sigma_{dc}\sigma_{opt}^{-1} = 37.4$.

PEDOT:PSS films fabricated by spin-coating as described in the Experimental Section. As seen, the EG-treated PEDOT:PSS films exhibit T_{550} and R_S values from 79% to 91% and 55 to 226 $\Omega\ sq^{-1}$, respectively; the corresponding values for ITO films are 92% and 14 $\Omega\ sq^{-1}$. The average thickness of each PEDOT:PSS layer is ~37 nm and, as expected, R_S and T_{550} decrease with increasing total thickness t. As is well known, the relation between T and R_S for transparent electrodes is given by[18,28]

$$T = \left(1 + \frac{Z_O}{2R_S}\frac{\sigma_{opt}}{\sigma_{dc}}\right)^{-2} \quad (2)$$

where $Z_0 = 377\ \Omega$ is the impedance of free space, and σ_{opt} and σ_{dc} are the optical and dc conductivities, respectively. By using Equation (2) to fit T_{550} and R_S vs. t of the PEDOT:PSS films, an excellent fit is obtained over the whole thickness range with $\sigma_{dc}\sigma_{opt}^{-1} = 37.4$ (see the inset of Figure 1). This value is larger than the minimum industry standard requirement of $\sigma_{dc}\sigma_{op}^{-1} = 35$,[18,28] indicating that these PEDOT:PSS films are suitable as transparent anodes in PHOLEDs.

Atomic force microscopy (AFM) images of the multilayered PEDOT:PSS and ITO films are shown in Figure S2 of the SI. The root-mean-square surface roughness R_{rms} of the treated PEDOT:PSS films with $t \approx 36$, 72, 114, and 149 nm are 2.0, 2.0, 2.5 and 3.1 nm, respectively. As seen, there were small aggregates on the surface of the treated PEDOT:PSS films; they are believed to be PEDOT-rich domains, as described elsewhere.[30] These R_{rms} values are significantly smaller than the 4.4 nm of the ITO films (Figure S2 (e)); the smoother PEDOT:PSS films likely improve the contact with the adjacent HTL, which may present another advantage of the PEDOT:PSS films over ITO for OLEDs.[11,19]

Prior to fabrication of the ITO-free PHOLEDs, PHOLEDs with an ITO anode were optimized. For this purpose, the combinatorial sliding-shutter technique was used. This enables fabrication of a two-dimensional (2-d) array of OLED pixels, where the thickness of two organic layers is varied systematically across the array, as described elsewhere.[29–30] Following fabrication of two 2-d combinatorial PHOLED arrays on an ITO anode, the following optimized device structure was achieved: glass/ITO (180 nm)/MoO_3 (1 nm)/MoO_3 (10 wt%):NPD (22.5 nm)/NPD (22.5 nm)/Ir(ppy)$_3$ (6 wt%):CBP (11 nm)/BPhen (34 nm)/LiF (1 nm)/Al (100 nm). The corresponding peak efficiencies are $\eta_{L,max} = 78\ Cd\ A^{-1}$, $\eta_{P,max} = 82\ lm\ W^{-1}$ and $\eta_{ext,max} = 24\%$ at a brightness $L = 117\ Cd\ m^{-2}$ and a drive voltage $V = 3.0$ V (see Figure S3 in SI). The turn-on voltage V_{on} (i.e., V at $L = 1\ Cd\ m^{-2}$), not only for the optimized PHOLEDs, but also for all the other 15 different PHOLEDs fabricated in the second 2-d array, was ~2.6 V. This value is very close to the thermodynamic limit (i.e., the emitted photon energy divided by the charge of an electron),[31] ~ 2.4 V. V_{on} is independent of the thickness of the Ir(ppy)$_3$ (6 wt%):CBP layer and BPhen layer, which may indicate that it is largely determined by the efficiency of hole injection and transport.[32] In addition, its proximity to the thermodynamic limit clearly suggests that using the MoO_3 (1 nm) HIL/MoO_3 (10 wt%):NPD/NPD HTL yields a nearly ideal Ohmic contact between the ITO and the HTL, minimizing the energy loss at the ITO/HTL interface and leading to PHOLEDs with better power efficiency.[33–37] These efficiencies of the optimized ITO-anode PHOLEDs are among the highest reported for any ITO-anode OLEDs devoid of outcoupling enhancement.[38–39] It is therefore an excellent reference for comparison with PEDOT:PSS-anode PHOLEDs described next.

The PEDOT:PSS-anode PHOLEDs with the following structure were fabricated and evaluated: glass/PEDOT:PSS (x nm)/MoO_3 (1 nm)/MoO_3 (10 wt%):NPD (22.5 nm)/NPD (22.5 nm)/Ir(ppy)$_3$ (6 wt%):CBP (11 nm)/BPhen (34 nm)/LiF (1 nm)/Al (100 nm), where $x \approx 36$, 72, 114 and 149 nm. Among these 4 different PEDOT:PSS-anode PHOLEDs, only the 2-layered 72 nm- and 3-layered 114 nm-thick PEDOT:PSS anodes yielded better performance than the corresponding ITO-anode PHOLEDs. This is clearly due to the relatively high R_S value (226 $\Omega\ sq^{-1}$) for the 1-layered 36 nm-thick and the low T_{550} value (79%) for the 4-layered 149 nm-thick PEDOT:PSS films. The high R_S limits the current injection and the low T_{550} reduces the light extraction efficiency, hampering the PHOLEDs' performance. Therefore, only the results for the 2-layered 72 nm- and 3-layered 114 nm-thick PEDOT:PSS-anode PHOLEDs are shown in **Figure 2**.

Figure 2a shows the electroluminescence (EL) spectra of PHOLEDs with 2- and 3- layered PEDOT:PSS anodes and ITO anode at a current density $J = 57\ mA\ cm^{-2}$. As seen, the spectra are nearly identical, peaking at ~514 nm (E_{Photon} ~ 2.4 eV), and clearly originating from Ir(ppy)$_3$, independent of the anode.

The brightness L and current density J vs. V are shown in Figures 2b and c. In both figures, the ITO-anode PHOLEDs show very steep L and J vs. V curves compared to the PEDOT:PSS-anode PHOLEDs, which is clearly due to the significantly higher R_S of the PEDOT:PSS films ($R_{S,2\ layers} = 115\ \Omega\ sq^{-1}$, $R_{S,3\ layers} = 72\ \Omega\ sq^{-1}$ vs. $R_{ITO} = 14\ \Omega\ sq^{-1}$). Comparing the 2-layered to the 3-layered PEDOT:PSS-anode PHOLEDs, the 2-layered shows slightly higher L, but lower J than the 3-layered device throughout the whole bias range, which is consistent with the higher T_{550} and R_S for the 2-layered PEDOT:PSS anode ($T_{550,2\ layers} = 87\%$, $T_{550,3\ layers} = 82\%$).

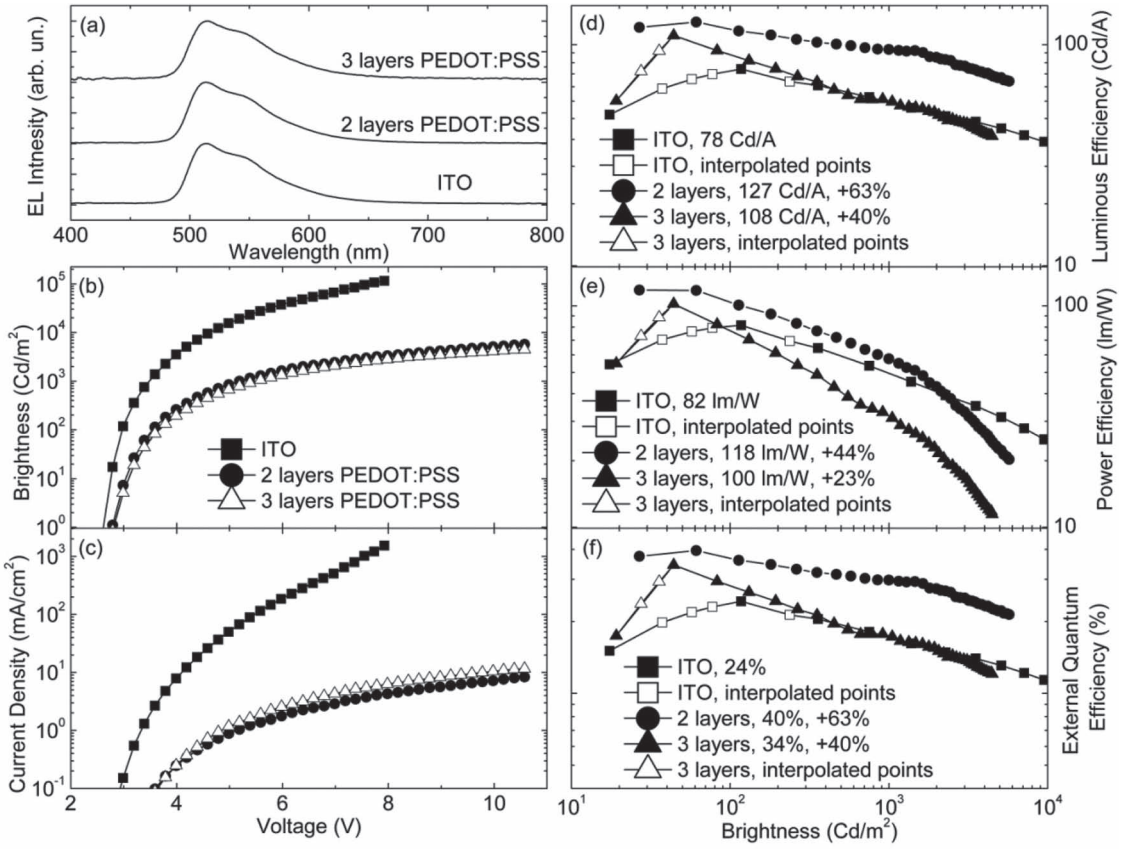

Figure 2. Comparison of device characteristics. (a) EL spectra, (b) *L* vs. *V*, (c) *J* vs. *V*, (d) η_L vs. *L*, (e) η_P vs. *L* and (f) η_{ext} vs. *L* of ITO-anode (black squares), 2-layered PEDOT:PSS-anode (red circles) and 3-layered PEDOT:PSS-anode (blue triangles) PHOLEDs. Open symbols are interpolated from the curves in (b) and (c).

The work function $\phi_{PEDOT:PSS}$ ~ 5.1 - 5.2 eV is higher than that of ITO (ϕ_{ITO} ~ 4.5–4.8 eV).[10,16–19,25,40] It was previously shown that V_{on} of the PEDOT:PSS-anode OLEDs is lower than that of ITO-anode OLEDs,[16,19] as expected from the respective ϕ_{anode} values. That is, the reduced V_{on} may be due to the higher $\phi_{PEDOT:PSS}$ that reduces the energy barrier for hole injection to the adjacent HTL.[10,16,19] However, in this study, V_{on} of the PEDOT:PSS- and ITO-anode PHOLEDs are comparable, and those of PEDOT:PSS-anode are only ~0.2 V higher than those of the ITO-anode devices ($V_{on,2\ layers} = V_{on,3\ layers}$ ~ 2.8 V; $V_{on,ITO}$ ~ 2.6 V). As mentioned above, a nearly perfect Ohmic contact is formed by using MoO_3 (1 nm) HIL/MoO_3 (10 wt%):NPD/NPD HTL. Under this condition, we believe that the difference $\Delta\phi$ between the different anodes is not the dominant factor determining V_{on}. Rather, the conductivity of the anode material becomes increasingly important. As seen in Figure 2c, at any given *V*, the corresponding *J* for the ITO-anode PHOLEDs is at least one order of magnitude larger than that of PEDOT:PSS-anode PHOLEDs. The $J_{ITO}J_{PEDOT:PSS}^{-1}$ ratio increases as the drive *V* increases, exceeding 100 at $V > 6.8$ V. This is clearly due to the higher resistance of PEDOT:PSS relative to ITO. This can also explain the relatively low maximum brightness L_{max} of the PEDOT:PSS-anode PHOLEDs compared to that of ITO-anode PHOLEDs, simply due to the limited injected charge carriers that form the light-emitting excited states.

While the electrical characteristics of the PHOLEDs with the PEDOT:PSS anodes are inferior to those of the PHOLEDs with the ITO anodes, calculating the efficiencies of the former points to the advantages of using the *multilayered* PEDOT:PSS. Figures 2d–f show plots of η_L, η_P and η_{ext} vs. *L* for the 2- and 3-layered PEDOT:PSS-anode and ITO-anode PHOLEDs. As clearly seen, the PEDOT:PSS-anode PHOLEDs show significantly better performance than the ITO-anode PHOLEDs. For the 3-layered PEDOT:PSS-anode PHOLEDs, $\eta_{L,max}$ = 108 Cd A^{-1}, $\eta_{P,max}$ = 100 lm W^{-1} and $\eta_{ext,max}$ = 34%. These values present a ~40% improvement in η_L and η_{ext} and a ~23% improvement in η_P over those of the ITO-anode PHOLEDs. Because of the higher T_{550} value for the 2-layered PEDOT:PSS films, the enhancement in device performance is more pronounced for the 2-layered PEDOT:PSS-anode PHOLEDs. The $\eta_{L,max}$ increased to 127 Cd A^{-1} and $\eta_{ext,max}$ to 40%; both are 63% higher than the ITO-anode PHOLEDs. The $\eta_{P,max}$ is improved to 118 lm W^{-1}, which is 44% higher than that of the ITO-anode devices. These efficiencies are among the highest reported to date for any ITO-free OLED. For both 2- and 3-layered PEDOT:PSS-based PHOLEDs, the relative improvement in η_P is much less than that in η_L and η_{ext}, e.g., 44% vs. 63% for the 2-layered and 23% vs. 40% for the 3-layered, respectively. This difference indicates that only a fraction of the optical improvement introduced by the PEDOT:PSS anode is realized in η_P. This is clearly due

to the low conductivity of the PEDOT:PSS anode that requires higher driving voltage. In addition, as seen in Figures 2d–f, the efficiency roll-off in η_L and η_{ext} is much less than that of η_P for PEDOT:PSS-anode PHOLEDs. For example, in the 2-layered PHOLEDs, at ~5000 Cd m^{-2} η_L and η_{ext} are still 56% of the $\eta_{L,max}$ and $\eta_{ext,max}$, but η_P has dropped to 20% of its peak value; the corresponding values for ITO PHOLEDs are 54% in η_L and η_{ext}, and 38% in η_P. This demonstrates that the efficiency roll-off in η_L and η_{ext} is comparable for both 2-layered PEDOT:PSS and ITO PHOLEDs, but in η_P it is much greater for the 2-layered, which, again, is due to the high resistivity of the PEDOT:PSS anode. This also explains the observation that η_L and η_{ext} of 2-layered PEDOT:PSS PHOLEDs is larger than those of ITO PHOLEDs throughout the whole brightness range, but η_P become less than that of ITO PHOLEDs around 3000 Cd m^{-2}. All of these observations suggest that further improving the optical and electrical properties of the PEDOT:PSS films and increasing the value of $\sigma_{dc}\sigma_{opt}^{-1}$ as close as possible to that of ITO (> 300) will result in not only even more efficient devices, but also a moderation of the efficiency roll-off. This may conceivably be achieved by modifying the PEDOT:PSS anode with additives other than EG.

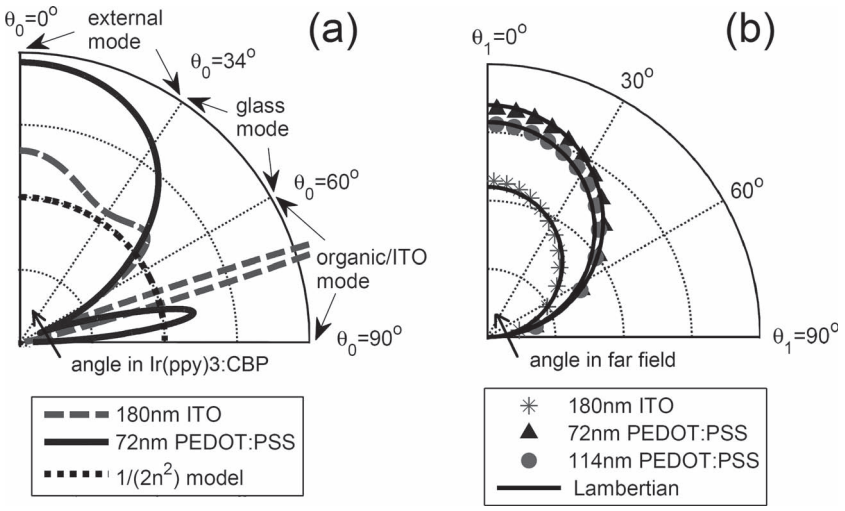

Figure 3. (a) Angular emission profiles of dipoles in $Ir(ppy)_3$:CBP in devices with ITO (dashed line) and PEDOT:PSS (solid line) anodes. The uniform angular emission profile assumed in the $1/(2n^2)$ model is also plotted as a dotted line for reference. (b) Angular emission profiles of the extracted light.

The optical enhancement obtained with the PEDOT:PSS anodes was simulated using a classical dipole model,[41–46] where an exciton embedded in the active layer is modeled as a point dipole, the emission of which is affected by the reflected electromagnetic waves inside a microcavity. According to the simulation, the enhanced light outcoupling in the devices with a PEDOT:PSS anode is attributed to the weak microcavity effect. We applied the Fresnel boundary conditions at all interfaces to each component plane wave, then solved the electromagnetic field inside the microcavity and thus obtained the angular emission profile of the dipoles as well.

In the following, two cases comparing the light outcoupling from ITO and PEDOT:PSS devices are described: (1) glass/ITO (180 nm)/organic layers (90 nm)/Al, and (2) glass/PEDOT:PSS (72 nm)/organic layers (90 nm)/Al. The emission profiles of the dipoles are plotted in **Figure 3**a as a function of the emission angle in $Ir(ppy)_3$:CBP-based devices; a uniform angular emission pattern assumed in the simple $1/(2n^2)$ model[42] is also plotted as a reference. The emitted light can be divided into 3 modes that are defined by the critical angles for total internal reflection at the air/glass ($\theta_0 = 34°$) and glass/organic ($\theta_0 = 60°$) interfaces:

(1) external modes that are extracted out of the device ($0° < \theta_0 < 34°$),
(2) substrate modes that are trapped in the glass for an ITO anode or in glass + PEDOT:PSS for a PEDOT:PSS anode ($34° < \theta_0 < 60°$; $n_{PEDOT:PSS}$ is very close to n_{gl}), and
(3) organic/ITO modes that are trapped in the ITO + organic layers for an ITO anode or only in organic layers for PEDOT:PSS anodes ($60° < \theta_0 < 90°$).

As Figure 3a shows, there is a strong coupling to organic/ITO waveguided modes (at the expense of the emitted light) in devices with ITO anodes at $\theta_0 > 70°$ (see the sharp peak that is out of scale). In comparison, the organic waveguided mode in devices with PEDOT:PSS anodes is suppressed and consequently the external mode is enhanced. The reason is that the two devices contain different organic waveguides. In ITO devices, since $n_{ITO} > n_{Org}$, the light is trapped in the organic + ITO layers, whose total thickness is 180 + 90 = 270 nm. In PEDOT:PSS devices, the light is only trapped in the organic layers, whose thickness is 90 nm. Thus, the organic waveguided modes are different for the two devices and the resulting coupling strength to them is also different.

Figure 3b shows the angular emission profiles of the outcoupled light, where θ_1 is the viewing angle in the far field. They resemble Lambertian profiles, in agreement with the observed profiles (see Figure S4 in the SI). The calculated relative enhancement of light outcoupling in the PEDOT:PSS device compared to the ITO one is ~56% at 514 nm, which is in good agreement with the experimental results.

We also simulated the ITO-based PHOLEDs' emitted intensity as a function of ITO thickness (see Figure S5 in the SI) by Fourier space solutions of Maxwell's equations in a scattering matrix (SM) formalism.[43] We found that the intensity of these PHOLEDs decreases continuously and substantially (by >25%) as the ITO thickness increases from 130 to 200 nm, which is a very interesting phenomenon that warrants further investigation.

We note that the efficiency of the PEDOT:PSS-anode PHOLEDs might be further enhanced by the addition of structures such as microlens arrays (μLAs) on the back side of the glass substrate, which will extract the light trapped in the glass.[7,9] As mentioned, the glass substrates used in the PEDOT:PSS- and ITO-anode PHOLEDs are identical. The angular emission profile of the PEDOT:PSS-anode devices is

Lambertian, as is the case for the ITO-anode devices. Since replacing ITO with PEDOT:PSS has no effect on the glass/air interface, we believe that embossing the recently reported uniform square μLAs[9] or the random scattering array based on polyethylene glycol:polystyrene blends[8] on the back side of PEDOT:PSS/glass, may further enhance η_{out} by up to 100%, strongly increasing device performance.

In conclusion, we have shown that ITO-free OLEDs with $\eta_{P,max}$ = 118 lm W^{-1}, without outcoupling-enhancing structures, can be realized. This enhanced performance of the multilayered PEDOT:PSS-anode PHOLEDs is largely the result of the advantageous optical properties of the polymer anode, which is strongly supported by detailed optical simulations. The results elucidate the underlying relationship between the polymer anode and device performance and highlight the strong roles of material/film thickness and treatment as well as the weak microcavity effect. They will consequently help in further enhancing the efficiencies of OLEDs. With its strongly improved device performance we believe that the multilayered highly conductive PEDOT:PSS films are promising for a bright future for ITO-free OLEDs. This is due not only to the resulting outstanding efficiencies they yield, but also to their flexibility and potential low cost.

Experimental Section

PEDOT:PSS (Clevios PH 1000) was purchased from H. C. Starck and used as the anode. MoO_3 was purchased from Sterm Chemicals; it was used as the hole injection material and p-dopant. NPD, the hole transport material, was purchased from H. W. Sands. CBP, the host material, was purchased from Luminescence Technology Corporation. $Ir(ppy)_3$, the green emitting material, was purchased from American Dye Source. BPhen was purchased from Sigma-Aldrich and used as the electron-transport and hole-blocking material. All materials were used as received.

Preparation and Characterization of PEDOT:PSS Films: PEDOT:PSS solutions were mixed with 6 vol.% EG. The resulting solutions were filtered with 0.45 μm syringe filters and spin-coated on precleaned and UV ozone treated glass substrates, which are identical to the glass substrates used for devices with an ITO anode. Single-layer PEDOT:PSS films were fabricated by spin coating at 3000 rpm for 30 s and annealing at 120 °C for 15 min. Immediately after annealing, they were immersed and cooled in an EG bath for 30 min, then spun at 3000 rpm for another 30 s to remove the EG solution. Next, the samples were annealed at 120 °C for another 15 min. For multilayer coatings of PEDOT:PSS, the next PEDOT:PSS layer was prepared in the same way described above on the existing PEDOT:PSS layer(s). After the PEDOT:PSS deposition was completed, the films were first baked at 120 °C for 1 h, then transferred into an Ar-filled glovebox (< 10 ppm O_2) and baked at 120 °C for another 1 h to remove residual water. We note that the EG and heating result in layers that remain intact following subsequent spin-coating of PEDOT:PSS layers, and the multilayered structure was essential for reduced sheet resistance, despite its reduced transparency. ITO substrates (Colorado Concept Coatings) with a sheet resistance of 14 Ω sq^{-1} and a transmittance of 92% were used for reference diodes.

Sheet resistances were measured using a four point probe setup with a source measurement unit (Keithley 200 and Fluke 8842A). The thickness of the PEDOT:PSS films was determined by scanning electron microscope images (Field Emission AmRay 1845) and the thickness of the ITO was determined by Ambios XP-100 profilometer. Transmittance was obtained using a spectrophotometer (Ocean Optics CHEM2000); the values given are at 550 nm and include the absorption by the glass substrate (~ 5%). The morphology of the films was obtained by AFM (model MM AFM-2 from Digital Instruments, employing tapping mode).

Fabrication and Characterization of OLEDs: All OLEDs were fabricated on the glass/PEDOT:PSS or the glass/ITO substrates in a thermal evaporation chamber within a glovebox with a base pressure of ~2 × 10^{-6} mbar. The cleaned ITO substrates were dried by blowing nitrogen and then treated in a UV ozone oven to increase the work function of the ITO and hence facilitate hole injection, as described elsewhere.[47] The two-dimensional OLED arrays were fabricated with a sliding shutter technique. MoO_3, NPD, CBP, $Ir(ppy)_3$, BPhen, LiF, and Al layers were deposited sequentially; the Al cathode was deposited through a shadow mask containing 1.5 mm diameter circular holes. Bias voltages across the OLEDs were supplied by a Kepco DPS 40-2M programmable power supply and the current was measured using a Keithley 2000 multimeter. As the voltage of the power supply could only be varied in 0.2 V increments, a few of the data points at low brightness shown in Figures 3(d)–3(f) were obtained by interpolating the values of *J* and *L* from the curves shown in Figure 3b and c. The OLEDs' brightness was measured using a Minolta LS110 luminance meter and the EL spectra were obtained using an Ocean Optics CHEM2000 spectrometer. The raw spectra were obtained in the "SCOPE" mode, but were corrected to the radiometrically calibrated mode; the spectra shown are the corrected spectra. The external quantum efficiency η_{ext} was calculated by using a method previously described.[48]

Supporting Information

Supporting Information is available from Wiley Online Library or from the author.

Acknowledgements

We thank Dr. Chun Xu for computational programs. This work was supported by the US Department of Energy, Basic Energy Sciences, Materials Sciences and Engineering Division, under Contract No. DE-AC 02-07CH11358.

Received: May 22, 2012
Revised: May 4, 2012
Published online: July 12, 2012

[1] C. W. Tang, S. A. Vanslyke, *Appl. Phys. Lett.* **1987**, *51*, 913.
[2] J. H. Burroughes, D. D. C. Bradely, A. R. Brown, R. N. Marks, K. Mackay, R. H. Friend, P. L. Burn, A. B. Holmes, *Nature* **1990**, *347*, 539.
[3] S. Reineke, F. Lindner, G. Schwartz, N. Seidler, K. Walzer, B. Lussem, K. Leo, *Nature* **2009**, *459*, 234.
[4] M. A. Baldo, D. F. O'Brien, Y. You, A. Shoustikov, S. Sibley, M. E. Thompson, S. R. Forrest, *Nature* **1998**, *395*, 151.
[5] C. Adachi, M. A. Baldo, M. E. Thompson, S. R. Forrest, *J. Appl. Phys.* **2001**, *90*, 5048.
[6] E. L. Williams, K. Haavisto, J. Li, G. E. Jabbour, *Adv. Mater.* **2007**, *19*, 197.
[7] K. Saxena, V. K. Jain, D. S. Mehta, *Opt. Mater.* **2009**, *32*, 221.
[8] R. Liu, Z. Ye, J.-M. Park, M. Cai, Y. Chen, E. Hellerich, K.-M. Ho, R. Shinar, J. Shinar, *Opt. Express* **2011**, *19*, A1272.
[9] J.-M. Park, Z. Q. Gan, W. Y. Leung, R. Liu, Z. Ye, K. Constant, J. Shinar, R. Shinar, K. M. Ho, *Opt. Express* **2011**, *19*, A786.
[10] M. Cai, T. Xiao, E. Hellerich, Y. Chen, R. Shinar, J. Shinar, *Adv. Mater.* **2011**, *23*, 3590.
[11] D. S. Hecht, L. B. Hu, G. Irvin, *Adv. Mater.* **2011**, *23*, 1482.
[12] A. M. Alfantazi, R. R. Moskalyk, *Miner. Eng.* **2003**, *16*, 687.
[13] M. A. Green, *Prog. Photovoltaics* **2009**, *17*, 347.

[14] D. R. Cairns, R. P. Witte, D. K. Sparacin, S. M. Sachsman, D. C. Paine, G. P. Crawford, R. R. Newton, *Appl. Phys. Lett.* **2000**, *76*, 1425.
[15] D. R. Cairns, G. P. Crawford, *Proc. IEEE* **2005**, *93*, 1451.
[16] K. Fehse, K. Walzer, K. Leo, W. Lovenich, A. Elschner, *Adv. Mater.* **2007**, *19*, 441.
[17] S. I. Na, S. S. Kim, J. Jo, D. Y. Kim, *Adv. Mater.* **2008**, *20*, 4061.
[18] Y. H. Kim, C. Sachse, M. L. Machala, C. May, L. Muller-Meskamp, K. Leo, *Adv. Funct. Mater.* **2011**, *21*, 1076.
[19] M. Cai, T. Xiao, R. Liu, Y. Chen, R. Shinar, J. Shinar, *Appl. Phys. Lett.* **2011**, *99*, 153303.
[20] M. W. Rowell, M. A. Topinka, M. D. McGehee, H. J. Prall, G. Dennler, N. S. Sariciftci, L. B. Hu, G. Gruner, *Appl. Phys. Lett.* **2006**, *88*, 233506.
[21] L. G. De Arco, Y. Zhang, C. W. Schlenker, K. Ryu, M. E. Thompson, C. W. Zhou, *Acs Nano* **2010**, *4*, 2865.
[22] J. Meiss, M. K. Riede, K. Leo, *Appl. Phys. Lett.* **2009**, *94*, 013303.
[23] M. G. Kang, M. S. Kim, J. S. Kim, L. J. Guo, *Adv. Mater.* **2008**, *20*, 4408.
[24] T. W. Koh, J. M. Choi, S. Lee, S. Yoo, *Adv. Mater.* **2010**, *22*, 1849.
[25] T. Xiao, W. Cui, J. Anderegg, J. Shinar, R. Shinar, *Org. Electron.* **2011**, *12*, 257.
[26] J. Ouyang, Q. F. Xu, C. W. Chu, Y. Yang, G. Li, J. Shinar, *Polymer* **2004**, *45*, 8443.
[27] H. Okuzaki, Y. Harashina, H. Yan, *Eur. Polym. J.* **2009**, *45*, 256.
[28] V. Scardaci, R. Coull, J. N. Coleman, *Appl. Phys. Lett.* **2010**, *97*, 023114.
[29] L. Zou, V. Savvate'ev, J. Booher, C. H. Kim, J. Shinar, *Appl. Phys. Lett.* **2001**, *79*, 2282.
[30] Z. Q. Gan, Y. Tian, D. W. Lynch, J. H. Kang, Q. H. Park, J. Shinar, *J. Appl. Phys.* **2009**, *106*, 094502.
[31] M. C. Gather, A. Kohnen, K. Meerholz, *Adv. Mater.* **2011**, *23*, 233.
[32] S. Lamansky, R. C. Kwong, M. Nugent, P. I. Djurovich, M. E. Thompson, *Org. Electron.* **2001**, *2*, 53.
[33] M. Kroger, S. Hamwi, J. Meyer, T. Riedl, W. Kowalsky, A. Kahn, *Org. Electron.* **2009**, *10*, 932.
[34] J. H. Lee, H. M. Kim, K. B. Kim, J. J. Kim, *Org. Electron.* **2011**, *12*, 950.
[35] C. Y. H. Chan, C. M. Chow, S. K. So, *Org. Electron.* **2011**, *12*, 1454.
[36] X. F. Qiao, J. S. Chen, X. L. Li, D. G. Ma, *J. Appl. Phys.* **2010**, *107*, 104505.
[37] G. H. Xie, Y. L. Meng, F. M. Wu, C. Tao, D. D. Zhang, M. J. Liu, Q. Xue, W. Chen, Y. Zhao, *Appl. Phys. Lett.* **2008**, *93*, 093305.
[38] G. F. He, M. Pfeiffer, K. Leo, M. Hofmann, J. Birnstock, R. Pudzich, J. Salbeck, *Appl. Phys. Lett.* **2004**, *85*, 3911.
[39] N. C. Erickson, R. J. Holmes, *Appl. Phys. Lett.* **2010**, *97*, 083308.
[40] Y. H. Zhou, F. L. Zhang, K. Tvingstedt, S. Barrau, F. H. Li, W. J. Tian, O. Inganas, *Appl. Phys. Lett.* **2008**, *92*, 233308.
[41] J. A. E. Wasey, W. L. Barnes, *J. Mod. Opt.* **2000**, *47*, 725.
[42] N. C. Greenham, R. H. Friend, D. D. C. Bradley, *Adv. Mater.* **1994**, *6*, 491.
[43] R. Biswas, C. Xu, W. Zhao, R. Liu, R. Shinar, J. Shinar, *J. Photon. Energy* **2011**, *1*, 011016.
[44] S. Mladenovski, S. Hofmann, S. Reineke, L. Penninck, T. Verschueren, K. Neyts, *J. Appl. Phys.* **2011**, *109*, 083114.
[45] L. Penninck, P. D. Visschere, J. Beeckman, K. Neyts, *Opt. Express* **2011**, *19*, 18558.
[46] M. Furno, R. Meerheim, S. Hofmann, B. Lussem, K. Leo, *Phys. Rev. B* **2012**, *85*, 115205.
[47] M. Cai, T. Xiao, Y. Chen, E. Hellerich, R. Liu, R. Shinar, J. Shinar, *Appl. Phys. Lett.* **2011**, *99*, 203302.
[48] H. Li, C. Zhang, D. Li, Y. Duan, *J. Lumin.* **2007**, *122–123*, 626.